Simultaneous optical model analyses of elastic scattering, breakup, and fusion cross section data for the ^{6}He+^{209}Bi system at near-Coulomb-barrier energies

B. T. Kim, W. Y. So, and S. W. Hong
Department of Physics and Institute of Basic Science, Sungkyunkwan University, Suwon 440-746, Korea

T. Udagawa
Department of Physics, University of Texas, Austin, Texas 78712
(Received 21 November 2001; published 2 April 2002)

Based on an approach recently proposed by us, simultaneous χ^2 analyses are performed for elastic scattering, direct reaction (DR), and fusion cross section data for the ^{6}He+^{209}Bi system at near-Coulomb-barrier energies to determine the parameters of the polarization potential consisting of DR and fusion parts. We show that the data are well reproduced by the resultant potential, which satisfies the proper dispersion relation. A discussion is given of the nature of the threshold anomaly seen in the potential.

DOI: 10.1103/PhysRevC.65.044616 PACS number(s): 24.10.−i, 25.70.Jj

A great deal of effort has recently been focused on studies of the so-called threshold anomaly [1,2] (rapid energy variation in the strength of the optical potential) in heavy-ion scattering induced, particularly, by very loosely bound projectiles such as ^{6}He [3], ^{6}Li [4–6], and ^{9}Be [7,8]. The experimental results accumulated so far indicate that the imaginary part of the optical potential, $W(r;E)$, extracted by the analysis of the elastic scattering data, does not show such an anomaly as is observed in the potentials for normal, tightly bound projectiles. For tightly bound projectiles, $W(r;E)$ at around the strong absorption radius $r=R_{sa}$ is found to decrease rapidly as the incident energy E falls below the Coulomb-barrier energy E_c, and eventually vanishes at some *threshold* energy E_0. Contrary to this, for loosely bound projectiles $W(R_{sa};E)$ remains large at energies even below E_c [3,5,6,8].

The reason for $W(R_{sa};E)$ being so large at low energies has been ascribed to the weak binding of the extra neutrons to the core nucleus, leading to breakup. In fact, the breakup cross sections have been measured for these projectiles [9–11], confirming that they are indeed large, even larger than the fusion cross sections at $E\sim E_c$. It was argued [1] that since the energy dependence of the polarization potential due to the breakup must be weak, one might not be able to observe a rapid energy variation in $W(r;E)$ when the breakup cross section is larger than the fusion cross section as for loosely bound projectiles.

It was pointed out sometime ago [12] that the threshold anomaly of $W(r;E)$ observed for tightly bound projectiles might originate from the coupling of the elastic and fusion channels. This is substantiated by the fact that the threshold energy E_0 of $W(r;E)$ [i.e., the energy where $W(r,E_0)=0$] agrees very well with that of the fusion cross section σ_F or, more precisely, the threshold energy of $S(E)\equiv\sqrt{E\sigma_F}$ [13]. It is thus natural that if the breakup cross section is larger than the fusion cross section and if one is concerned only with the total $W(r;E)$, the rapid change in the fusion cross section and the anomaly would not show up clearly in the total $W(r;E)$.

It may thus be interesting to decompose the total $W(r;E)$ into the direct reaction (DR) and fusion parts, $W_D(r;E)$ and $W_F(r;E)$, respectively, and determine them separately [14]. The aim of the present study is to make such a determination of $W_D(r;E)$ and $W_F(r;E)$ by performing simultaneous χ^2 analyses of elastic scattering, DR (breakup), and fusion cross section data. We take the ^{6}He+^{209}Bi system, for which data are available not only for elastic scattering [3], but also for breakup [9] and for fusion [15]. Following Ref. [3], we identify the breakup cross section with the DR cross section. Optical model analyses of the elastic scattering and total reaction cross section data have already been presented in Refs. [3,16,17]. The present analysis is thus an extension of the previous studies.

The optical potential U we use has the following form:

$$U=U_C(r)-[V_0(r)+V(r;E)+iW(r;E)], \tag{1}$$

where $U_C(r)$ is the Coulomb potential, whose radius parameter is fixed as a standard value of $r_c=1.25$ fm, and $V_0(r)$ is the Hartree-Fock part of the potential, while $V(r;E)$ and $W(r;E)$ are, respectively, real and imaginary parts of the so-called polarization potential [18] that originates from couplings to reaction channels. $W(r;E)$ is assumed to have a volume-type fusion and a surface-derivative-type DR part [14]. Explicitly, $V_0(r)$ and $W(r;E)$ are given, respectively, by

$$V_0(r)=V_0 f(X_0) \tag{2}$$

and

$$W(r;E)=W_F(r;E)+W_D(r;E)$$
$$=W_F(E)f(X_F)+4W_D(E)a_D\frac{df(X_D)}{dR_D}, \tag{3}$$

where $f(X_i)=[1+\exp(X_i)]^{-1}$, with $X_i=(r-R_i)/a_i$ ($i=0$, D and F), is the usual Woods-Saxon function. The real part of the polarization potential is also assumed to have DR and fusion parts: $V(r;E)=V_F(r;E)+V_D(r;E)$. Each real part may be generated from the corresponding imaginary potential by using the dispersion relation [1]

$$V_i(r;E)=V_i(r;E_s)+\frac{E-E_s}{\pi}\mathrm{P}\int_0^\infty dE'\frac{W_i(r;E')}{(E'-E_s)(E'-E)}, \tag{4}$$

where P stands for the principal value and $V_i(r;E_s)$ is the value of the potential at a reference energy $E=E_s$. Later, we will use Eq. (4) to generate the final real polarization potentials $V_F(r;E)$ and $V_D(r;E)$, after $W_F(r;E)$ and $W_D(r;E)$ have been fixed from χ^2 analyses. Note that the breakup cross section may include contributions from both Coulomb and nuclear interactions, which implies that the direct reaction potential includes both effects.

V_0 in Eq. (2) may have an energy dependence coming from the nonlocality due to the knockon-exchange contribution. We ignore such effects, however, in the present study, as they are expected to be small for heavy-ion scattering [18], and simply use the potential determined for the $\alpha+{}^{209}$Bi system at $E=22$ MeV [19], assuming that all the unusual features of the scattering may be described by the polarization part of the potential, particularly by the DR part. The parameters used for $V_0(r)$ are $V_0=100.4$ MeV, $r_0=1.106$ fm, and $a_0=0.54$ fm.

The unusual behavior of the elastic scattering and DR data for loosely bound projectiles can most dramatically be seen in plots of the ratios of the elastic differential cross section $(d\sigma_E/d\Omega)$ and the DR cross section $(d\sigma_D/d\Omega)$ to the Rutherford scattering cross section $(d\sigma_c/d\Omega)$, i.e.,

$$P_i\equiv\frac{d\sigma_i}{d\Omega}\Big/\frac{d\sigma_c}{d\Omega}=\left(\frac{d\sigma_i}{d\sigma_c}\right)\quad(i=E\text{ or }D), \tag{5}$$

as a function of the distance of the closest approach D (or the reduced distance d) [20,21], which is related to the scattering angle θ by

$$D=d(A_1^{1/3}+A_2^{1/3})=\frac{1}{2}D_0\left(1+\frac{1}{\sin(\theta/2)}\right), \tag{6}$$

with

$$D_0=\frac{Z_1Z_2e^2}{E}.$$

Here D_0 is the distance of the closest approach in a head-on collision (s wave). Further, (A_1,Z_1) and (A_2,Z_2) are the mass and charge of the projectile and target ions, respectively, and E is the incident energy in the center-of-mass system.

In Fig. 1, we present such plots for two incident energies of $E=18.5$ and 21.9 MeV [9]. As seen, P_E is close to unity for large d, but starts to decrease at an unusually large distance of $d=2.2$ fm $(\equiv d_I$, interaction distance). This value is much larger than the usual value of $d_I\approx1.6$ fm for normal, tightly bound projectiles [22]. On the other hand, it is remarkable that the sum P_E+P_D remains close to unity until d becomes as small as $d\approx1.7$ fm, implying that the absorption in the elastic channel up to this distance, and the unusual character of the scattering data, is due to the breakup. For $d\leqslant1.7$ fm, P_E+P_D becomes smaller than unity, which may be ascribed due to fusion; in fact, in our recent paper [22], we have demonstrated that this is indeed the case.

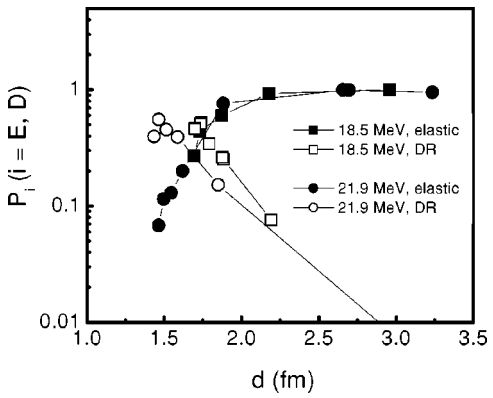

FIG. 1. The experimental elastic and DR probabilities P_E and P_D, respectively, as functions of the reduced distance d for the ^{6}He+^{209}Bi system at $E_{\mathrm{c.m.}}=18.5$ and 21.9 MeV. The data are taken from Ref. [9]. The thin lines connecting P_i $(i=E$ and $D)$ values are only to guide the eyes.

Since the theoretical cross sections are not very sensitive to the real polarization potential, we tentatively treat it in a rather crude way in carrying out χ^2 analyses; we simply assume $V_i(r;E)$ has the same radial shape as the imaginary part $W_i(r;E)$: $V_i(r;E)=V_i(E)[W_i(r;E)/W_i(E)]$, $V_i(E)$ being the strength of the real potential. We then carry out χ^2 analyses treating $W_F(E)$ and r_D as adjustable parameters, keeping all other parameters fixed as $V_F=3.0$ MeV, $r_F=1.40$ fm, $a_F=0.55$ fm, $V_D=0.25$ MeV, $W_D=0.40$ MeV, and $a_D=1.25$ fm. In fixing these other parameters, preliminary analyses of the data were done with many sets of parameter values. The above values are found as a possible set of the optimal values. The necessity of varying a_D or r_D as a function of E has been shown in previous studies [3,16], and in the present work we take r_D as a variable parameter as a function of E, because choosing a_D as an adjustable energy-dependent parameter led to much larger χ^2 values. In the χ^2 analyses, data for elastic scattering, angle-integrated total DR, and fusion cross sections at $E=14.3$, 15.8, 17.3, 18.6, and 21.4 MeV are employed.

The values of $W_F(E)$ and $r_D(E)$ fixed from the χ^2 analyses are presented in Fig. 2 as open and solid circles, respectively. Each set of circles can be well represented by [in MeV and fm, respectively, for $W_F(E)$ and $r_D(E)$]

$$W_F(E)=\begin{cases}0 & \text{for } E\leqslant15.4,\\ 1.25(E-15.4) & \text{for } 15.4<E\leqslant18.5,\\ 4.00 & \text{for } 18.5\leqslant E,\end{cases} \tag{7}$$

and

$$r_D(E)=\begin{cases}1.730 & \text{for } E\leqslant14.0,\\ 1.730-0.03(E-14.0) & \text{for } 14.0<E\leqslant21.4,\\ 1.508 & \text{for } 21.4\leqslant E.\end{cases} \tag{8}$$

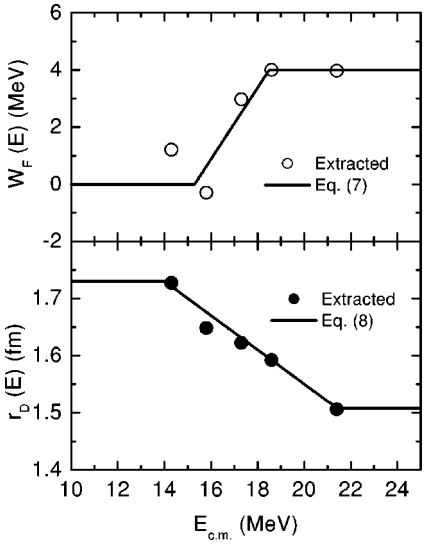

FIG. 2. The values of $W_F(E)$ (upper panel) and $r_D(E)$ (lower panel) extracted from the χ^2 analyses are plotted as the open and solid circles, respectively. The solid lines represent Eqs. (7) and (8).

Note that the threshold energy $E_0=15.4$ MeV, at which $W_F(E)=0$, is set equal to that of the linear representation of $S(E)=\sqrt{E\sigma_F}\propto(E-E_0)$ discussed earlier. Kolata *et al.* [15] found the value to be 15.4 MeV, which is used in Eq. (7). At this moment, we have no experimental data to fix on r_D values below 14.0 MeV and above 21.4 MeV. Thus, in Eq. (8), we tentatively set $r_D(E)$ to be constant as 1.73 fm for $E\leqslant 14.0$ fm and 1.508 fm for $E\geqslant 21.4$ MeV. Note that the values of $r_D(E)$ at $E=18.6$ and 21.4 MeV agree well with those determined by Mohr [16].

For a tightly bound system such as the $^{16}O+^{208}Pb$ system, no such energy dependent r_D was needed in order to reproduce the observed data [22]; only a slowly varying energy-dependent W_D was enough to reproduce them. The reason why r_D needs to be energy-dependent may be due to the change in the relative importance between the Coulomb and nuclear interactions. At the lower incident energies, Coulomb contributions become relatively more important, causing r_D to be larger. A somewhat similar energy dependence of the imaginary parts of the potentials is reported in Ref. [17].

Equations (7) and (8), together with other parameters used for $W_F(r;E)$ and $W_D(r;E)$ as mentioned above, completely fix the imaginary parts of the potential in the energy range between $E=14.0$ and 21.4 MeV. In order to display the energy dependence of the potentials, we present in the lower panel of Fig. 3 the values of $W_F(r;E)$, $W_D(r;E)$, and the sum $W(r;E)=W_F(r;E)+W_D(r;E)$ at a strong absorption radius $r=R_{sa}=13.0$ fm. It is remarkable that $W_F(R_{sa};E)$ plotted as the dotted line exhibits a threshold anomaly (strong energy variation) similar to that observed for tightly bound projectiles. However, $W_D(R_{sa};E)$ plotted as the dashed line is rather flat as a function of E and has a magnitude much larger (by about a factor of 5) than $W_F(R_{sa};E)$. Therefore, the threshold anomaly in $W_F(R_{sa};E)$ does not manifest itself in the total $W(R_{sa};E)$ plotted as the solid line.

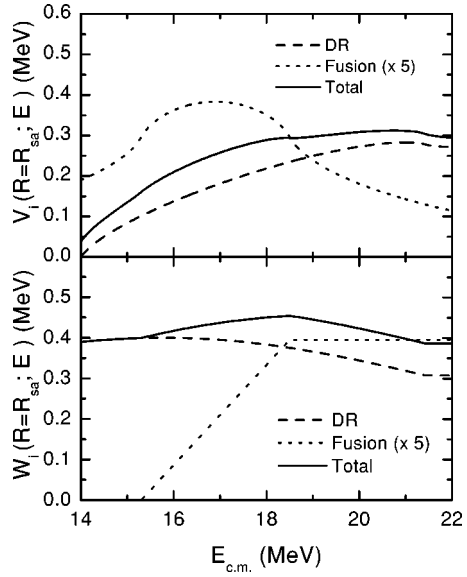

FIG. 3. The real (upper panel) and the imaginary (lower panel) parts of fusion (dotted line) and DR (dashed line) potentials as functions of E at the strong absorption radius $r=R_{sa}=13.0$ fm. The sums of fusion and DR potentials are plotted as the solid lines. The real parts of the potentials are calculated by using Eq. (9) for $V_F(E)$ and Eq. (12) for $V_D(E)$.

In order to generate the real part of the polarization potential by using dispersion relations, we need to know the imaginary potential in the entire range of E. Equation (7) with $a_F=0.55$ fm and $r_F=1.40$ fm is enough for calculating $W_F(r;E)$ in the entire E range. For the fusion potential, since the geometrical parameters are energy independent, the dispersion relation is reduced to that for the strength parameters $V_F(E)$ and $W_F(E)$, and the closed form for the expression has already been obtained [1] as

$$V_F(E)=V_s(E_s)+\frac{1}{\pi}W_F(E_b)[\,\epsilon_b\ln|\epsilon_b|-\epsilon_a\ln|\epsilon_a|\,], \quad (9)$$

where

$$\epsilon_a=\frac{(E-E_a)}{(E_b-E_a)}, \quad \epsilon_b=\frac{(E-E_b)}{(E_b-E_a)}, \quad (10)$$

with $E_a=15.4$ MeV and $E_b=18.5$ MeV. The value chosen for $V_s(E_s)$ is 3.0 MeV at $E_s=18.5$ MeV.

For $W_D(r;E)$, some care must be taken with the magnitude. To do the initial χ^2 analyses, we used $W_D=0.4$ MeV with $a_D=1.25$ fm in fixing the $r_D(E)$ values as given by Eq. (8). The constant value of $W_D(E)=0.4$ MeV, however, cannot be used at very low energies, since the DR cross sections are expected to be extremely small in that energy region. The systematics of the data suggests that σ_D may become essentially zero for $E\leqslant 10$ MeV. We thus assume that $W_D(E)$ increases linearly from zero at 10 MeV to the value of 0.4 MeV at $E=14.0$ MeV. The strength $W_D(E)$ and the radius $r_D(E)$ parameters in the entire energy range E can then be rewritten as

$$W_D(E)=\begin{cases}0.0,\\ 0.1(E-10.0),\\ 0.40,\\ 0.40,\end{cases}$$

$$r_D(E)=\begin{cases}1.730 & \text{for } E\leqslant 10.0,\\ 1.730 & \text{for } 10.0\leqslant E\leqslant 14.0,\\ 1.730-0.03(E-14.0) & \text{for } 14.0\leqslant E\leqslant 21.4,\\ 1.508 & \text{for } 21.4\leqslant E.\end{cases} \tag{11}$$

Together with $a_D=1.25$ fm, Eq. (11) now defines $W_D(r;E)$ in the whole range of E.

In generating the real part of the DR potential, $V_D(r;E)$, by using the dispersion relation, we introduce an additional simplification of approximating the energy dependence of $W_D(r;E)$ between $E=14.0$ and 21.4 MeV, where $r_D(E)$ changes with E. We assume $W_D(r;E)$ to be a quadratic function of E at each radial point r: $W_D(r;E)=a+b(E-E_b)+c(E-E_b)^2$. Note that a, b, and c depend on r. We have confirmed that the approximation is accurate. Once this is done, the integration over E involved in Eq. (4) can be carried out analytically and one can get a closed form of $V_D(r;E)$,

$$\begin{aligned}V_D(r;E)=&V_s(r;E_s)+\frac{1}{\pi}W_D(r;E_b)[\epsilon_b\ln|\epsilon_b|-\epsilon_a\ln|\epsilon_a|]\\&+\frac{1}{\pi}[W_D(r;E_c)-W_D(r;E_b)][\epsilon_c'\ln|\epsilon_c'|-\epsilon_b'\ln|\epsilon_b'|]\\&+\frac{2}{\pi}[W_D(r;E_c)+W_D(r;E_b)-2W_D(r;E_m)]\\&\times[\epsilon_c'\epsilon_b'(\ln|\epsilon_c'|-\ln|\epsilon_b'|)+\epsilon_b'],\end{aligned} \tag{12}$$

where ϵ_a and ϵ_b have the same form as defined in Eq. (10) with $E_a=10.0$ MeV and $E_b=14.0$ MeV and

$$\epsilon_b'=\frac{(E-E_b)}{(E_c-E_b)},\quad \epsilon_c'=\frac{(E-E_c)}{(E_c-E_b)}, \tag{13}$$

with $E_c=21.4$ MeV and $E_m=(E_b+E_c)/2$.

Using the polarization potentials thus generated we perform the final calculations for elastic scattering, total DR, and fusion cross sections and present the results in Figs. 4 and 5 in comparison with the data. The data are fairly well reproduced by the calculations. The final calculated cross sections are essentially the same as those obtained in the initial χ^2 analysis, implying that the calculated cross sections do not sensitively depend on the real polarization potential, as we assumed in carrying out the χ^2 analysis. We note that the fits to the elastic scattering and reaction cross sections (sum of the DR and fusion cross sections) are essentially the same as those obtained in Ref. [3]. The fit to the elastic scattering data at the lowest energy $E=14.3$ MeV is the worst among those shown in Fig. 4, but can be improved if we carry out a χ^2 analysis including only the elastic scattering data as the data to be reproduced. We made such an analysis, finding that the data were very well reproduced with $r_D=1.93$ fm, much larger than $r_D=1.72$ fm obtained earlier. The DR cross section calculated with this $r_D=1.93$ fm, however, turned out to be $\sigma_D=540$ mb, about 3 times larger than the experimental value. This implies that one cannot improve the simultaneous fit to both the elastic and DR data any further.

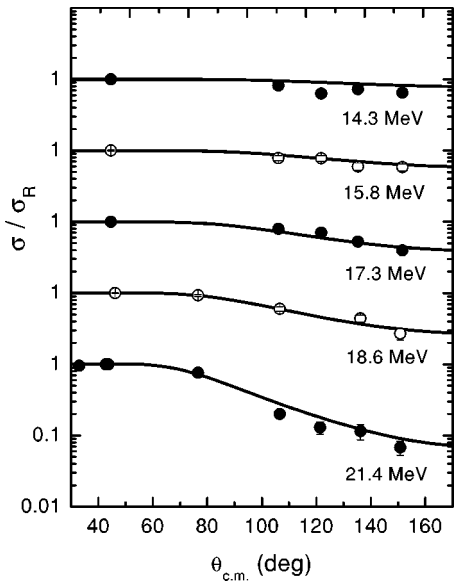

FIG. 4. The ratios of the elastic scattering cross sections to Rutherford cross sections, calculated with our final optical potential for the ^{6}He+^{209}Bi system in comparison with the experimental data. The data are taken from Ref. [3].

Much interest has been drawn recently to the question of whether a large breakup of loosely bound projectile enhances or reduces the fusion cross section [23]. There are two competing physical effects involved: one is the coupling with the breakup channel which lowers the fusion barrier and thus enhances the fusion cross section. The other is the removal of the flux from the elastic into the breakup channel which should reduce the fusion cross section.

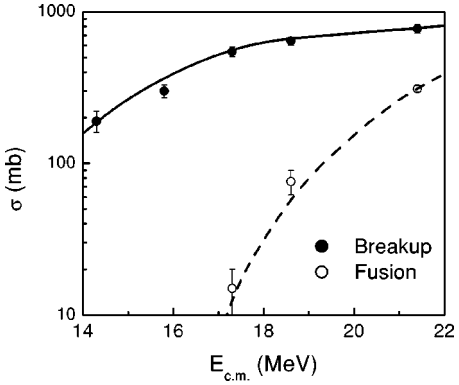

FIG. 5. The calculated DR and fusion cross sections with our final optical potential for the ^{6}He+^{209}Bi system in comparison with the experimental data. The data are taken from Refs. [3,15].

TABLE I. Various ratios of fusion cross sections.

$E_{\mathrm{c.m.}}$ (MeV)	$\sigma_F(V_D=0)/\sigma_F$	$\sigma_F(W_D=0)/\sigma_F$	$\sigma_F(V_D=W_D=0)/\sigma_F$
14.3	0.97	1.10	1.06
15.8	0.86	1.22	1.04
17.3	0.82	1.41	1.13
18.6	0.83	1.51	1.23
21.4	0.91	1.50	1.38

In the present treatment, the above two competing effects are described by means of the real $[V_D(r;E)]$ and imaginary $[W_D(r;E)]$ parts of the DR potential. The effects can thus be quantitatively estimated by carrying out the calculations of the fusion cross sections excluding either one of V_D and W_D or both, and by comparing the resultant fusion cross sections to the full calculation results. Indeed, we calculated σ_F by setting only V_D equal to 0, only W_D equal to 0, and both V_D and W_D equal to 0 and took the ratios of thus calculated σ_F to the final theoretical σ_F shown in Fig. 5. Such ratios are given in Table I. As seen, when we set $V_D=0$, the resultant ratios become smaller than unity, showing that V_D indeed enhances σ_F. The magnitude of the enhancement factor is, however, rather small, at most 20%. As expected, when we set $W_D=0$, the ratios become larger than unity, which means that the flux loss due to W_D reduces the fusion cross section. The reduction factor amounts up to 50%, larger than the enhancement factor due to V_D. Therefore, the net effect is a reduction in the fusion cross section. This is seen in the numbers listed in the last column of Table I, which are all larger than unity. An interesting feature here is that the reduction factor increases as the incident energy increases. This tendency may be understood from what we have discussed earlier that breakup takes place more inside the nucleus with increasing E and thus the region where the flux is lost in the elastic channel overlaps more with the region where fusion takes place. At extremely low energy of $E=14.3$ MeV, though the breakup cross section is still very large, the effect on the fusion cross section is small. This is due to the fact that at this energy breakup is dominated by the Coulomb interaction and thus causes very little effects on fusion.

In summary, we have carried out simultaneous χ^2 analyses of elastic scattering, DR (breakup), and fusion cross sections for the ^{6}He$+^{209}$Bi system at near-Coulomb-barrier energies within the framework of an optical model that introduces two types of imaginary potentials, for DR and fusion, and determined the parameters of these potentials. The results indicate that the fusion potential exhibits a threshold anomaly very similar to that observed for tightly bound projectiles, but the magnitude of the fusion potential at around the strong absorption radius is much smaller than the imaginary DR potential that does not show such an anomaly. Therefore, the resulting total imaginary potential does not show the anomaly.

The authors sincerely thank Professor J. J. Kolata for kindly sending numerical values of the data his group took. The authors also wish to express their sincere thanks to Professor W. R. Coker for kindly reading the manuscript and comments. One of the authors (B.T.K.) acknowledges support by the Korea Research Foundation (Grant No. KRF-2000-DP0085).

[1] C. C. Mahaux, H. Ngo, and G. R. Satchler, Nucl. Phys. **A449**, 354 (1986); **A456**, 134 (1986).
[2] M. A. Nagarajan, C. C. Mahaux, and G. R. Satchler, Phys. Rev. Lett. **54**, 1136 (1985).
[3] E. F. Aguilera *et al.*, Phys. Rev. C **63**, 061603(R) (2001).
[4] M. A. Tiede, D. E. Trckha, and K. W. Kemper, Phys. Rev. C **44**, 1698 (1991).
[5] N. Keeley, S. J. Bennett, N. M. Clarke, B. R. Fulton, G. Tungate, P. V. Drumm, M. A. Nagarajan, and J. S. Lilly, Nucl. Phys. **A571**, 326 (1994).
[6] A. M. M. Maciel *et al.*, Phys. Rev. C **59**, 2103 (1999).
[7] S. B. Moraes *et al.*, Phys. Rev. C **61**, 064608 (2000).
[8] C. Signorini *et al.*, Phys. Rev. C **61**, 061603(R) (2000).
[9] E. F. Aguilera *et al.*, Phys. Rev. Lett. **84**, 5058 (2000).
[10] G. R. Kelly *et al.*, Phys. Rev. C **63**, 024601 (2001).
[11] C. Signorini *et al.*, in *Proceedings of the International Conference BO2000*, edited by D. Vretenar (World Scientific, Singapore, 2000).
[12] T. Udagawa, M. Naito, and B. T. Kim, Phys. Rev. C **45**, 876 (1992).
[13] P. H. Stelson, Phys. Lett. B **205**, 190 (1988); P. H. Stelson, H. J. Kim, M. Beckerman, D. Shapira, and R. L. Robinson, Phys. Rev. C **41**, 1584 (1990).
[14] B. T. Kim, M. Naito, and T. Udagawa, Phys. Lett. B **237**, 19 (1990).
[15] J. J. Kolata *et al.*, Phys. Rev. Lett. **81**, 4580 (1998).
[16] P. Mohr, Phys. Rev. C **62**, 061601(R) (2000).
[17] An analysis which introduces W_D and W_F by separating the total W into two parts with a sharp cutoff radius was recently reported in the APS Meeting by Aguilera and Gomez-Camacho: E. F. Aguilera and A. Gomez-Camacho, Bull. Am. Phys. Soc. **46**, 84 (2001).
[18] G. R. Satchler and W. G. Love, Phys. Rep. **55**, 183 (1979).
[19] A. R. Barnett and J. S. Lilly, Phys. Rev. C **9**, 2010 (1974).
[20] R. Bass, *Nuclear Reactions with Heavy Ions* (Springer-Verlag, New York, 1980).
[21] G. R. Satchler, *Introduction to Nuclear Reactions* (Wiley, New York, 1980), p. 41.
[22] B. T. Kim, W. Y. So, S. W. Hong, and T. Udagawa, Phys. Rev. C **65**, 044607 (2002).
[23] See Ref. [15], and references cited therein.